Catalysis Today 154 (2010) 237–243

Contents lists available at ScienceDirect

Catalysis Today

journal homepage: www.elsevier.com/locate/cattod

Distribution of carbon deposits on reduced Co/Y-zeolite catalysts for Fischer–Tropsch synthesis

Dong-Keun Lee*, Dul-Sun Kim, Tae-Han Kim, Young-Kyung Lee, Su-Eon Jeong, Ngoc Thuan Le, Mi-Jung Cho, Sonia Devi Henam

Dept. of Chemical and Biological Engineering, Environmental Biotechnology National Core Research Center (EBNCRC), Environmental and Regional Development Institute, BK21 Graduate Education Program for Environmental Core Technology, Gyeongsang National University, 900 Gajwa-dong, Jinju-city, Gyeongnam, Republic of Korea

ARTICLE INFO

Article history:
Available online 22 April 2010

Keywords:
Co/Y-zeolite
Fischer–Tropsch synthesis
Chemisorptions
CO hydrogenation

ABSTRACT

A new simple characterization method was employed to investigate the formation of carbon deposits in reduced Co/Y zeolites. The method was based on temperature programmed surface reaction (TPSR) between adsorbed carbon deposits and hydrogen. Together with other characterization methods of FMR, TEM and H_2 chemisorption, CO hydrogenation reaction was performed on Co/Y zeolite catalysts, and the changes in CO hydrogenation activity and selectivity with metal distributions were also investigated. Especially the studies have discussions about the selectivity pattern of cobalt clusters within Y-zeolite cages and large cobalt metal aggregates on the external surface of the zeolites.

The catalyst having most of cobalt metal clusters inside the zeolite cages showed much more selective synthesis of C_3 and C_4 products than the other catalysts. It is suggested that the lower hydrogenating ability induced the enhanced chain propagation and the chain growth was terminated by the surface sites of cobalt clusters.

1. Introduction

The catalytic hydrogenation of carbon monoxide is one of the most extensively studied catalytic reactions, and is known to give broad range of products. Recent interest for CO hydrogenation, however, does give great attention to the control of product distribution [1–12], which can be achieved by using new CO hydrogenation catalysts which are able to avoid the conventional Schultz–Flory distribution. For this purpose finely dispersed metal clusters encapsulated by zeolite cages have received considerable attention because they can offer several advantages (molecular sieving selectivity, polyfunctional activity, etc.) over other supported metal catalysts such as silica- and alumina-supported ones. Cobalt clusters, prepared by reduction of Co (II) ions exchanged into A- and Y-zeolites, produced propylene as the sole hydrocarbon product under well-defined conditions [5]. Main products were C_4 olefins on finely dispersed cobalt and iron clusters in Y-zeolite [8]. On iron, cobalt and ruthenium clusters in Y-zeolite short chain hydrocarbons in the C_1–C_9 range were produced probably due to the shape selective behaviors [6,12]. Finely dispersed metal clusters inside zeolite cages, however, may become mobile during treatment procedures enough to move through the cages until they can agglomerate into large, immobile aggregates at the exterior surface of zeolites [13,14]. Since simultaneous presence of finely dispersed metal clusters inside zeolite pores and large metal aggregates outside the zeolite crystals was first reported to occur for reduced NiX zeolite [15], bidisperse metal distributions have been observed for reduced CuY [16–18], AgY [18,19] and NiY zeolites [18,20,21].

The trapping of catalytic active species into a selective penetrable shell to form micro-encapsulated or nano-encapsulated catalysts with a core–shell structure has been reported, utilizing zeolite or carbon shells [33–38].

Metal distributions of the reduced metal-zeolite catalysts are of great importance because they can have a major effect on the activity and selectivity of catalyzed reactions. Characterization of metal distribution in reduced metal–zeolite catalysts has been made conventionally either through a consecutive temperature programmed reaction/oxidation procedure or through magnetic characterization techniques.

In this paper, a new simple characterization method was employed to investigate cobalt metal distribution in reduced Co/Y zeolites. The method was based on temperature programmed surface reaction (TPSR) between adsorbed carbon monoxide and hydrogen. Together with other characterization methods of ferromagnetic resonance (FMR), transmission electron microscopy (TEM) and H_2 chemisorption, CO hydrogenation reaction was performed on this characterized catalysts, and the changes in CO hydrogenation activity and selectivity with metal distributions were also investigated. Especially concentrated studies and discussions were given to the selectivity pattern of cobalt clusters within Y-zeolite cages and large cobalt metal aggregates outside the zeolites.

* Corresponding author. Tel.: +82 55 751 5386; fax: +82 55 753 1806.
E-mail address: d-klee@gsnu.ac.kr (D.-K. Lee).

0920-5861/$ – see front matter © 2010 Elsevier B.V. All rights reserved.
doi:10.1016/j.cattod.2010.03.053

Table 1
Treatment conditions of Co/Y-zeolite catalysts.

Symbol	Treatment temperature (°C)	Linear heating rate (°C/min)	Treatment time (h)
A	500	2	18
B	500	20	72
C	700	20	24
D	700	20	168

2. Experimental

2.1. Catalysts

Cobalt clusters in NaY-zeolite were prepared through the metal carbonyl introduction method followed by the decomposition to zero-valent metals. The catalysts were prepared by physically dispersing cobalt carbonyl ($CO_2(Co)_8$) dissolved in n-pentane on the zeolite (Stream Chemicals) having a unit cell composition of $Na_{54.9}[(AlO_2)_{54.9}(SiO_2)_{137.1}]$. The zeolite was dehydrated in vacuo at 450 °C. The impregnation took place in an evacuated, sealed cell over a period of 12 h at −10 °C. The mixture was then warmed slowly to room temperature *in vacuo* over a period of 2 h and was maintained under a dynamic vacuum (10^{-6} Torr) for another 24 h. Three different catalysts having 6, 8 and 10 wt% cobalt loadings were prepared, and all subsequent manipulations were performed in a glove box with argon atmosphere. Prepared catalysts were treated with hydrogen at four different conditions designated by the symbols in Table 1. The treated catalyst was identified in terms of (cobalt loading wt%) – (treatment condition), and the marks will be used in the rest of the text.

2.2. Characterization

Ferromagnetic resonance (FMR) spectra of cobalt metals were recorded at X-band frequencies on a Varian E-4 spectrometer. DPPH (2,2-dipenyl-1-picrylhydrazylg) was used as a standard to determine *g*-values. Quartz sample tube was designed for *in situ* operation.

Transmission electron microscopy (TEM) was done with JEOL 200CX microscope using 160 keV electrons.

Static hydrogen adsorption measurements were performed in a conventional Pyrex glass volumetric adsorption apparatus at 298 K. Gas uptakes were determined by extrapolating the straight portion of the total and reversible isotherms to zero pressure and the irreversible H_2 gas uptakes were taken as adsorption capacities of the cobalt metals.

2.3. Temperature programmed surface reaction (TPSR)

0.2 g catalyst sample was loaded in a quartz tubular microreactor and then treated with hydrogen at different conditions. After cooling the catalyst under helium stream to room temperature, appropriate amount of carbon monoxide was introduced to saturate metal surfaces *via* a calibrated injection port. Two different experiments of TPSR were carried out. For the first experiment, CO was preadsorbed at room temperature, and TPSR between the preadsorbed CO and flowing H_2 (20 cm^3/min) was conducted. For the second experiment, CO was dissociated at 270 °C to deposit surface carbon through the reaction $2CO \rightarrow C + CO_2$, and TPSR between surface carbon and flowing H_2 (20 cm^3/min) was done. The exit gas stream, mainly methane, was analyzed continuously as the reactor temperature increased linearly at 5 °C/min.

2.4. CO hydrogenation

CO hydrogenation reactions were performed in a quartz tubular microreactor under atmospheric pressure. The reactor was designed for *in situ* operation without contact with atmosphere. The H_2/CO ratio was maintained at 2 and the reaction temperature varied from 230 to 390 °C. Products were separated in a 4 ft × 1/8 in. Chromosorb 102 column and were analyzed with a Hewlett Packard 5710 A gas chromatograph with TCD and FID detectors connected

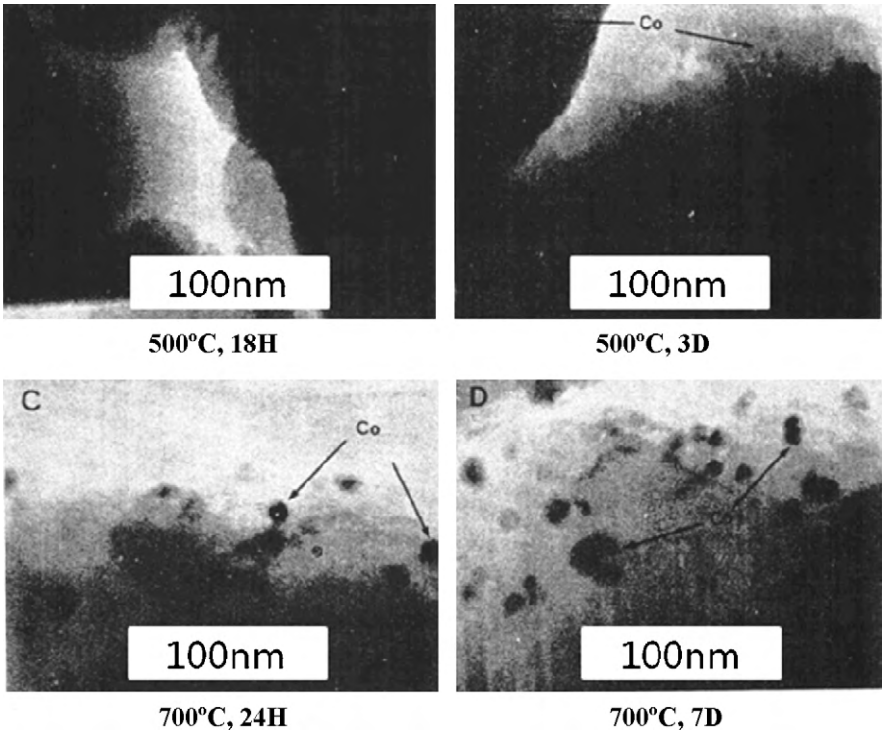

Fig. 1. TEM photographs of 10 wt% Co/Y-zeolite catalysts with treatment condition.

in series. The column temperature was temperature-programmed for the complete separation of olefins and paraffins.

3. Results and discussion

3.1. Characterization

Changes in the size and location of cobalt metal particle with treatment condition were investigated by TEM, and four representative TEM photographs of the treated 10 wt% Co/Y-zeolites are shown in Fig. 1. In 10-A catalyst (Photograph A) no cobalt metals of detectable size could be observed. In this case cobalt metals seem to be of a size less than that of faujasite supercage (=1.3 nm), and most metals are believed to exist within zeolite pores as finely dispersed clusters. When looking 10-A catalyst in more detail with TEM (Fig. 2), finely dispersed cobalt particles could be seen within zeolite pores.

Photograph B is an image of the sample which underwent a more severe treatment condition B. Many cobalt particles of about 6.0 nm became to appear. When the treatment was done under condition C (photograph C), the growth of metal particles is remarkable, and large metal particles are shown to locate outside the zeolite crystals. This indicates that more and more metal migrated out of the zeolites pores and agglomerated at the exterior surface of zeolite crystals as bulky particles.

When 10-C catalyst was held at 700 °C for another 6 days (photograph D), extremely large particles was found to form due to the prolonged sintering of particles in 10-C catalyst.

Ferromagnetic resonance spectra of cobalt metals are shown in Fig. 3. Nearly symmetric and narrow spectra ($\angle H$ = 750 G) appear at the g-value of 2.17 for the catalysts treated at condition A. Since the g-value and peak-to-peak line width did vary only slightly with detection temperature (−150 to 300 °C), which is a typical feature of the very small superparamagnetic particles [22,23], cobalt metals in the A catalysts seem to locate within the pores of Y-zeolite as finely dispersed clusters.

In 10-B catalyst, however, the spectrum became asymmetric and peak-to-peak line width increased significantly. This indicates that cobalt metals grew further enough to show magnetic anisotropies [20,22,24].

As the treatment condition becomes more severe (10-C, D catalysts in this case), the FMR spectra showed very irregular forms. The shape or size distribution of cobalt metals in the catalysts will not be uniform, which was previously evidenced from TEM photographs.

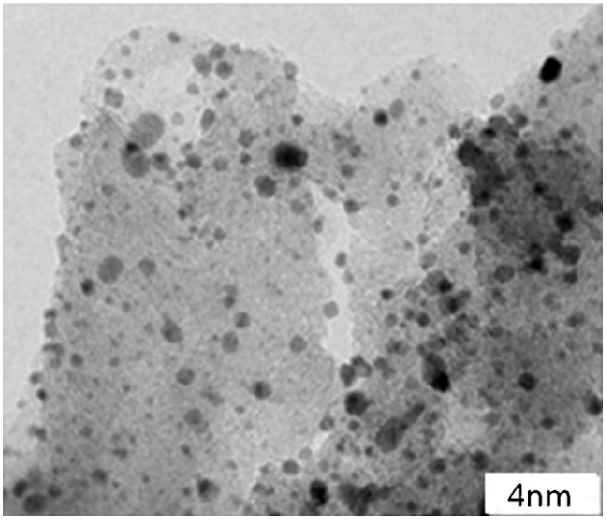

Fig. 2. Detailed TEM photograph of 10-A catalyst.

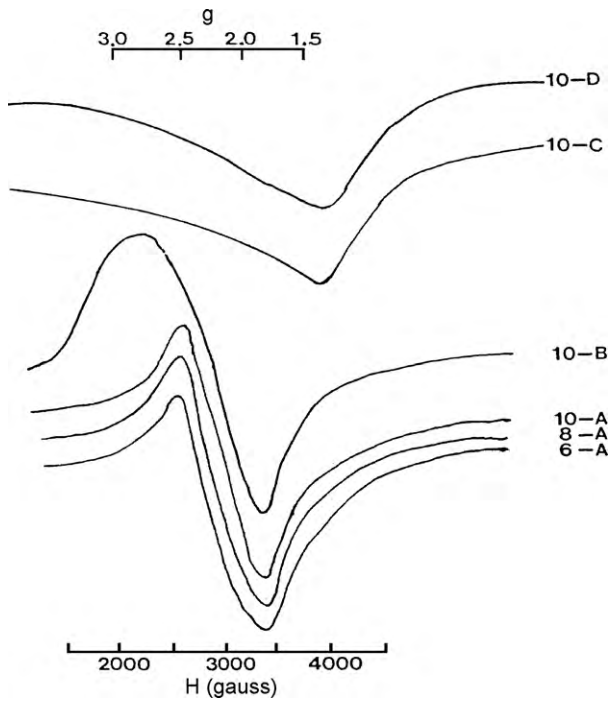

Fig. 3. FMR spectra of reduced Co/Y-zeolite catalysts.

Aforementioned results from TEM and FMR indicate that the size and location of cobalt metals do vary with treatment conditions. Finely dispersed cobalt clusters inside zeolite pores (Catalyst A) migrate out of zeolite pores and agglomerate outside the zeolites crystals showing bidisperse metal distributions (Catalyst B), and continuous metal migrations result in the formation of large cobalt metal particles at the exterior surface of zeolite crystals (Catalysts C and D).

3.2. TPSR

TPSR spectra between preadsorbed CO and flowing H_2 in 10 wt% Co/Y-zeolite catalysts are shown in Fig. 4. Catalysts treated at various conditions have very different TPSR spectra of methane. The main peak appears at about 570 °C in 10-A catalyst where most cobalt metals were believed to locate inside zeolite pores as finely dispersed clusters, while in 10-D catalyst having bulky cobalt metal

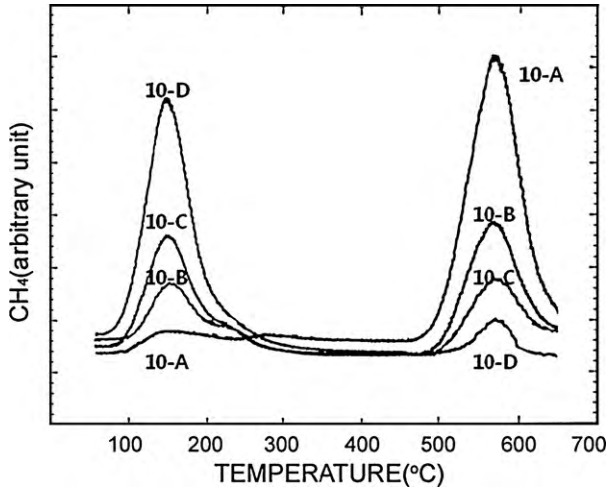

Fig. 4. TPSR spectra of CO preadsorbed of 10 wt% Co/Y-zeolite catalysts at 25 °C.

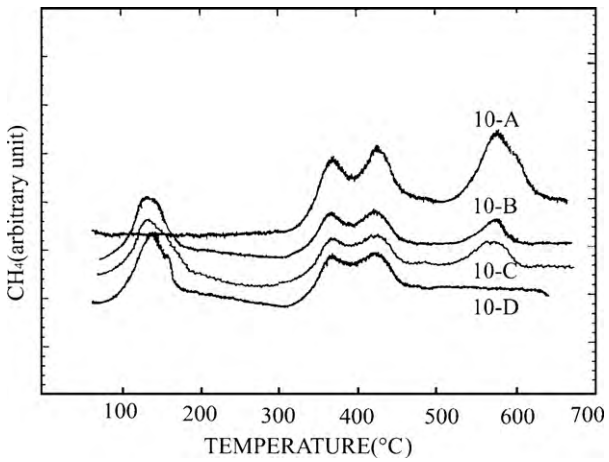

Fig. 5. TPSR spectra of 10 wt% Co/Y-zeolite catalysts predeposited by surface carbon at 270 °C.

aggregates outside the zeolite much lower temperature peak at around 150 °C becomes dominant. This distinct difference in TPSR spectra with treatment conditions can be employed successfully to investigate the cobalt metal locations in Y zeolite. Two representative peaks appearing at around 150 °C and at around 570 °C will be assigned to be α and β peak respectively in the rest of the text.

As more cobalt metal clusters migrate out of zeolite pores and agglomerate to bulky aggregates at the exterior surface of zeolite crystals through the treatment condition A to D, simultaneous increase and the corresponding decrease in α and β peak respectively is observed from TPSR spectra.

The differences in the major TPSR peak temperature with cobalt metal locations may be argued to be due to one or more of the followings; different dissociation rate of adsorbed CO, different rate of reaction between surface carbon and hydrogen, or diffusional restriction by molecular dimension zeolite pores. The diffusional effect, however, is considered to be minor because the diffusion process of methane is relatively fast in faujasite channels.

The same amounts of carbon monoxide as those introduced in Fig. 4 were injected on the surface of 10 wt% Co/Y-zeolite catalysts at 270 °C, which is thought to be high enough for surface carbon to form on the transition metal surface via CO dissociation reaction ($2CO \rightarrow C + CO$) [25,26]. Subsequent to CO injection, CO and CO_2 concentrations at the exit of the reactor were monitored with a mass spectrometer. In proportion to the decrease in CO concentration, CO_2 was formed due to CO dissociation, which was an evidence for the formation of surface carbon.

The above catalysts having surface carbon were then cooled slowly to room temperature under helium stream, and TPSR spectra were obtained by flowing hydrogen on the catalysts through the same procedure as that in Fig. 4. As shown in Fig. 5 the main peaks of 10-B, C and D catalysts shift slightly to lower temperature, but new peaks do appear at about 350–450 °C through the hydrogenation of predeposited surface carbons.

Adsorbed hydrogen is known to react with the surface carbon readily and thus remove the surface carbon formed by CO dissociation as methane [26–28]. Atomically dispersed platinum was, however, reported to be inactive to H_2 chemisorption [29], and the suppression of H_2 chemisorption manifests itself from the results of the chemisorbed hydrogen uptakes (Table 2). Even though 10-A catalyst has much higher metal surface exposed when compared with the other catalysts, the H_2 uptakes of 10-A catalyst is extremely lower than those of the other catalysts. Both the different CO dissociation rates and the different rates of reaction between surface carbon and hydrogen are believed to play important roles simultaneously for the differences in the major TPSR peak temperature with the location of cobalt metal particles.

Table 2
H_2 uptakes of the reduced Co/Y-zeolite catalysts.

Catalyst	H_2 uptakes (μmol/gcat.)
10-A	0.9
10-B	92.0
10-C	123.0
10-D	76.0
8-A	0.9
8-B	78.0
8-C	110.0
8-D	66.0
6-A	0.6
6-B	63.0
6-C	87.0
6-D	52.0

Anyway, the formation of the two distinct α and β TPSR peaks can be employed as a simple method to discriminate whether cobalt metals are placed within zeolite pores or outside the zeolite crystals. α-Peak represents the dominant existence of bulky cobalt metal particles outside the zeolite crystals, while the finely dispersed cobalt metal particles within zeolite pores evolve CH_4 mainly at β-peak.

3.3. Activity

The A catalysts were discussed in Section 3.1 to have finely dispersed metal clusters inside zeolite pores. And through the gradual treatment of catalysts from A to D condition more and more metal clusters inside zeolite cages migrated out of the pores until they agglomerate into large, immobile aggregates at the exterior surface of zeolite crystals. Table 3 shows sharp changes in activity with metal distributions. About 100-fold differences in activity are observed between catalysts A and D. Since cobalt metal particles of the catalyst D were much larger in size than those of the catalyst A, metal surface sites will be much more abundant in catalyst A. Fu and Bartholomew [30] also observed that CO hydrogenation activity increases with increasing cobalt metal particle size, and they suggested it to be due to the structure sensitive nature of CO hydrogenation on cobalt catalysts, i.e., more active lower coordination surface sites. The activity difference in Table 3 can be ascribed to the particle size differences. Poor hydrogen chemisorptions on finely dispersed cobalt clusters may also be another reason for the intrinsic activity difference. Even though catalyst A had much higher metal surfaces exposed when compared with the other catalysts, the hydrogen chemisorptions on catalyst A was extremely poorer than the other catalysts. When the surface hydrogen concentration

Table 3
Changes in CO hydrogenation activity of the reduced Co/Y-zeolite catalysts (270 °C, $H_2/CO = 2$).

Catalyst	Rate × 10^8 (mol/gcobalt s)
10-A	26.0
10-B	1670.0
10-C	2350.0
10-D	3150.0
8-A	18.0
8-B	850.0
8-C	1450.0
8-D	1970.0
6-A	12.0
6-B	680.0
6-C	1030.0
6-D	1460.0

Table 4
Hydrocarbon product distribution of the reduced Co/Y-zeolite catalysts (270 °C, $H_2/CO = 2$).

Catalyst	Product distribution (wt%)					
	C_1	C_2	C_3	C_4	C_5	C_6
10-A	34.7	14.1	26.3	18.3	6.6	–
10-B	49.2	20.0	18.3	10.1	2.0	0.4
10-C	68.4	15.7	10.2	5.1	0.6	–
10-D	70.2	13.6	8.3	6.4	1.5	–
8-A	32.4	12.5	18.8	22.6	3.7	–
8-B	51.1	19.6	15.7	7.6	3.9	2.1
8-C	70.1	13.3	9.4	5.2	1.8	0.2
8-D	73.3	12.9	7.1	4.6	2.1	–
6-A	26.4	9.6	23.1	38.8	2.1	–
6-B	48.3	21.3	16.5	8.4	3.5	2.0
6-C	64.8	16.2	13.7	4.9	0.4	–
6-D	69.5	15.4	11.8	3.1	0.2	–

is low, most surfaces will be covered by carbon monoxide and the rate of hydrogenation will be suppressed greatly. The great activity differences in Table 3 seem to have occurred from the changes in cobalt metal particle size on one hand and the relative surface hydrogen concentrations on the other hand.

3.4. Hydrocarbon product distributions

Table 4 shows hydrocarbon product distributions of the catalysts having different metal distributions. The products are represented as the number of carbon atoms per molecule and their respective concentrations are listed as weight percentage. The difference appears to be significant in product distribution. In catalyst A where most cobalt atoms located inside zeolite cages as finely dispersed metal clusters C_3 and C_4 hydrocarbons are produced in significant quantities, while in the other catalysts the main product is methane, showing a conventional Schulz–Flory distribution [31,32]. This indicates that cobalt clusters within zeolites cages are potential candidate good for selectivity control. But when the cobalt clusters migrated out of zeolite cages and agglomerated into large metal particles at the exterior surface of zeolite crystals, metal–zeolite catalysts are no longer expected to be able to control product selectivity. Figs. 6 and 7 show the ratio of olefins

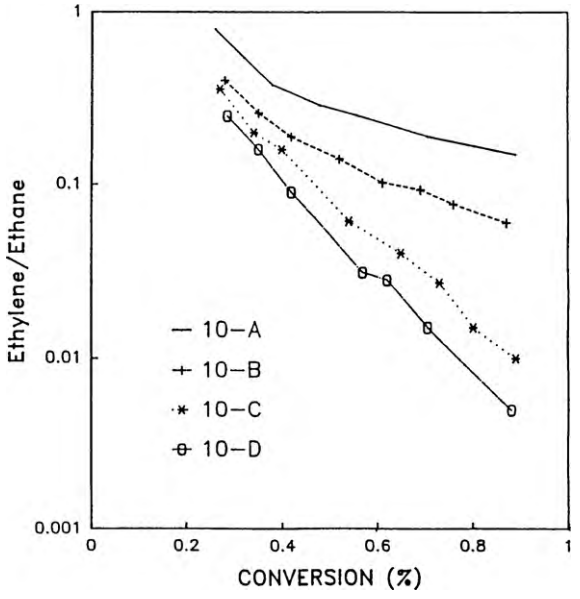

Fig. 6. Changes in ethylene/ethane ratio with conversion (reaction condition: 270 °C, $H_2/CO = 2$).

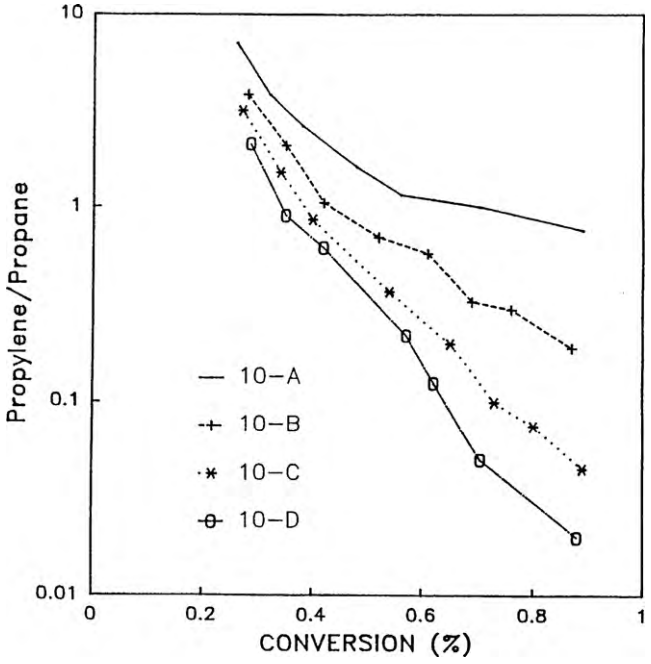

Fig. 7. Changes in propylene/propane ratio with conversion (reaction condition: 270 °C, $H_2/CO = 2$).

to paraffins for C_2 and C_3 species respectively versus conversion. The samples A–D show different values here as well. The ratios decrease significantly with increasing conversion, indicating that ethylene and propylene are the primary products which can either be hydrogenated to the corresponding paraffins or propagate to higher hydrocarbons. Since the hydrocarbon product distribution did vary only slightly with conversion, the decreased amount of the olefins with increasing conversion is then believed mainly to be hydrogenated to the corresponding paraffins rather than be incorporated to chain propagation step. As shown in Figs. 6 and 7 the olefin ratio decreases over catalyst 10-A less with increasing conversion than it does over samples 10-B to 10-D catalysts. Therefore the primarily formed olefins on catalysts A are known to be more difficult to be hydrogenated to the corresponding paraffins. This seems to be due to the extremely low hydrogen chemisorption uptake on 10-A catalyst (Table 2). Additionally the olefin to paraffin ratios of 10-A catalysts are always greater than those of the other catalysts all through the conversion, which provides a further evidence for the aforementioned extremely poor surface hydrogen concentration on the 10-A catalyst.

3.5. Catalyst A

Attention was focused especially on the catalysts A showing rather selective synthesis of C_3 and C_4 hydrocarbons, and efforts were made to interpret the unusual product distributions in the catalysts. Dependence of the hydrocarbon selectivities can be discussed on the basis of the reaction mechanisms. Carbon monoxide can be either dissociated to form methane preferentially or can be inserted in a CH_x–Co bond to give higher C_2^+ hydrocarbons. The previous TPSR results showed that not only the dissociation rate of the adsorbed carbon monoxide, but also the rate of the subsequent reaction between surface carbon and hydrogen to methane was much slower on the finely dispersed cobalt clusters within zeolite cages. These phenomena are undoubtedly believed to play an important role for the selective hydrocarbon product distribution in catalyst A. Rapid hydrogenation of carbon-containing surface intermediates will terminate the chain propagation of the inter-

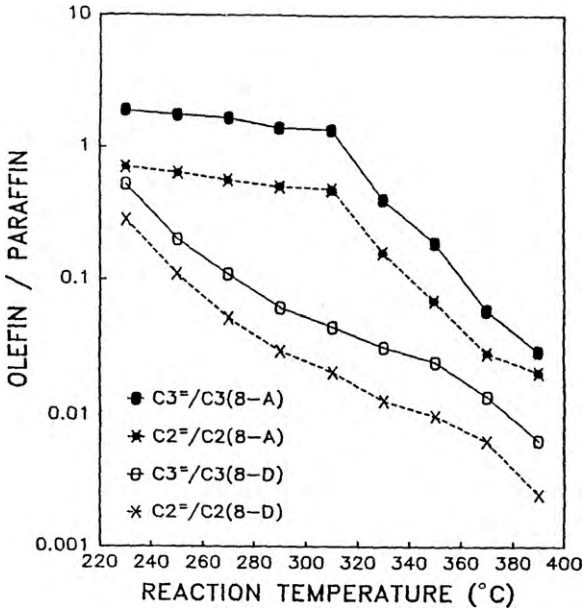

Fig. 8. Changes in olefin/paraffin ratio with reaction temperature (conversion = 0.55%, $H_2/CO = 2$).

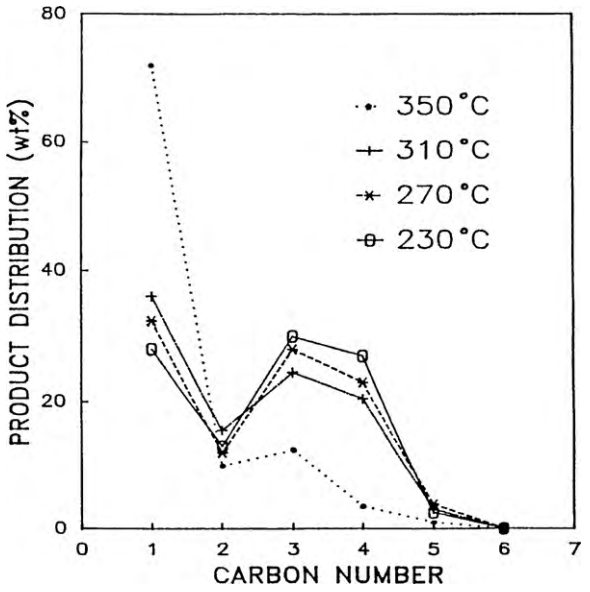

Fig. 9. Hydrocarbon product distribution with reaction temperature for 8-A catalyst (conv. = 0.55%, $H_2/CO = 2$).

mediates. Due to the termination of chain propagation methane is produced mainly. and this process will produce mainly methane. On the contrary the slow hydrogenation rate will provide the enhanced chain propagation probability for the CH_x–Co bond. The slow hydrogenation rate of the surface intermediates catalyst A manifests itself from the results in Fig. 8 where the changes in olefin to paraffin ratio with reaction temperature are plotted. In conventional Fischer–Tropsch catalysts the production of olefinic hydrocarbons decreases sharply with increasing reaction temperature, and the 8-D catalyst in Fig. 8 comes under this case. In the 8-A catalyst, however, the ratio decreases slightly up to 310 °C, and this seems to be due to the aforementioned suppressed hydrogen chemisorptions on the A catalysts.

From the TPSR results and the changes in olefin to paraffin ratio with reaction temperature (Fig. 8) it can be postulated easily that lower hydrogenating ability provides the higher chain propagation probability. The postulation becomes evident when the plots of 8-A catalyst in Fig. 8 are compared with the charges in hydrocarbon product distribution of the 8-A catalyst with reaction temperature (Fig. 9). C_3 and C_4 hydrocarbons are still produced in large quantities up to 310 °C where the changes in olefin to paraffin ratio were slight, while above 310 °C, where olefin to paraffin ratio decreased drastically, the product distribution shows a distinctly different pattern, i.e., the conventional Schulz–Flory distribution. This implies that the lower hydrogenating ability of 8-A catalyst must be linked closely with the selective hydrocarbon distribution of the catalyst.

Above discussions for the slow hydrogenation ability are believed to explain the higher chain propagation probability in the A catalysts. But the selective formation of C_3 and C_4 hydrocarbons on A catalysts cannot be fully explained in this manner, because the higher propagation ability cannot inevitably accompany the selective production of C_3 and C_4 hydrocarbons. In other words C_5 and/or other higher hydrocarbons may also be produced significantly through the enhanced chain propagation ability of the catalyst A.

For the selective production of C_3 and C_4 hydrocarbons the chain growth of the surface intermediates must be stopped at the corresponding surface to have free access to go in and out.

Surface metal atom ensembles of the very small spherical cobalt clusters can be assumed to be responsible for the selective production of C_3 and C_4 hydrocarbons. The domain of surface sites of the small cobalt clusters will not induce further growth of surface chain to C_5 and C_6 hydrocarbons, and may be particularly suitable for C_3 and C_4 chains. The selective production of C_3 and C_4 hydrocarbons in A catalysts is explained by the suggestion that the lower hydrogenating ability by the suppressed hydrogen chemisorption induced the enhanced chain propagation and the chain growth were terminated at C_3 and C_4 states by the narrow surface sites of cobalt clusters.

4. Conclusions

The effect of metal distribution in reduces CoY–zeolite catalysts on the activity and selectivity of CO hydrogenation was investigated.

Temperature programmed surface reaction (TPSR) between the adsorbed carbon monoxide and hydrogen was shown to be useful for the interpretation of bidisperse metal distribution. The lower temperature TPSR peak (α peak) was for the large metal aggregate outside the zeolite crystals, and higher temperature one (β peak) represented the finely dispersed cobalt clusters inside zeolite pores. The differences in the main TPSR peak temperature with metal locations seem to result from the simultaneous difference in CO dissociation rate and hydrogenation rate of surface carbon.

About 100-fold differences in activity with metal distributions were observed, which may result from both metal size effect and relative surface hydrogen concentration.

The catalyst A having most of cobalt metal clusters inside the zeolite cages showed much more selective synthesis of C_3 and C_4 products than the other catalysts. It is suggested that the lower hydrogenating ability induced the enhanced chain propagation and the chain growth was terminated by the surface sites of cobalt clusters in the catalyst A.

Acknowledgement

This work was supported by a grant from the KOSEF/MOST to the Environmental Biotechnology National Core Research Center (grant #: R15-2003-012-02002-0).

References

[1] M.A. Vannice, Catal. Rev. Sci. Eng. 14 (1976) 153.
[2] J. Falbe, New Synthesis with Carbon Monoxide, Springer Verlag, Berlin, 1980.
[3] H.H. Nijs, P.A. Jacobs, J.J. Vendock, J.B. Uytterhoeven, Chem. Soc. Commun. 4 (1979) 180.
[4] H.H. Nijs, P.A. Jacobs, J.B. Uytterhoeven, J. Chem. Soc. Commun. 23 (1979) 1095.
[5] D. Fraenkel, B.C. Gates, J. Am. Chem. Soc. 102 (1980) 2478.
[6] D. Ballivet-Tkatchenko, N.D. Chau, H. Mozzanega, M.C. Roux, I. Tkatchenko, Am. Chem. Soc. Symp. Ser. 152 (1981) 187.
[7] D. Ballivet-Tkatchenko, G. Coudurier, N.D. Chat, Stud. Sur. Sci. Catal. 12 (1982) 123.
[8] L.F. Nazer, G.A. Ozin, F. Hugues, J. Godber, J. Mol. Catal. 21 (1983) 313.
[9] Y.W. Chem, H.T. Wang, J.G. Goodwin Jr., J. Catal. 83 (1983) 415.
[10] S.L. Suib, K.C. Mcmahen, L.M. Tau, C.O. Bemmett, J. Catal. 89 (1984) 20.
[11] I.R. Leith, J. Catal. 91 (1985) 283.
[12] H.H. Nijs, P.A. Jacobs, J.J. Verdonck, J.B. Uytterhoeven, Stud. Surf. Sci. Catal. 4 (1979) 479.
[13] P.A. Jacobs, Stud. Surf. Sci. Catal. 12 (1982) 71.
[14] Kh.M. Minachev, G.V. Antoshin, E.S. Shpire, Yu.A. Yusofovs, Proceedings of the 6th International Congress Catalysis, vol. 2, London, 1977, p. 621.
[15] W. Romanovskii, Z. Anorg. Chem. 47 (1967) 741.
[16] R.G. Herman, J.H. Lunsford, H. Beyer, P.A. Jacobs, J.B. Uytterhoeven, J. Phys. Chem. 79 (1975) 2388.
[17] P.A. Jacobs, M. Tielen, L.P. Linart, H. Nijs, J.B. Uytterhoeven, H. Beyer, J. Chem. Soc. Faraday I 72 (1976) 2793.
[18] P.A. Jacobs, M. Tielen, J.P. Linart, H. Nijs, J.B. Uytterhoeven, J. Chem. Soc. Faraday I 731 (1977) 745.
[19] H. Beyer, P.A. Jacobs, J.B. Uytterhoeven, J. Chem. Soc. Faraday I 72 (1976) 674.
[20] P.A. Jacobs, H. Nijs, J. Vendock, E.G. Derouane, J.P. Gilson, A. Simoens, H. Beyer, J. Chem. Soc. Faraday I 75 (1979) 1196.
[21] A. Simoens, E.G. Derouane, Growth and Properties of Metal Clysters. Studies in Surface Science and Catalysis, vol. 4, Elsevier, Amsterdam, 1980, p. 201.
[22] M. Che, M. Richard, D. Olivier, J. Chem. Soc. Faraday I 76 (1980) 1526.
[23] V.K. Sharma, A. Baiker, J. Chem. Phys. 75 (15) (1981) 5596.
[24] A.J. Simoens, E.G. Derouane, R.T.K. Baiker, J. Catal. 75 (1982) 175.
[25] J.G. McCarty, H. Wise, J. Catal. 57 (1978) 406.
[26] R.W. Joyner, M.W. Roberts, Chem. Phys. Lett. 29 (1974) 447.
[27] C.H. Bartholomew, Catal. Rev. Sci. Eng. 24 (1982) 67.
[28] D.C. Gardner, C.H. Bartholomew, Ind. Eng. Chem. Prod. Res. Dev. 20 (1981) 80.
[29] T. Kubo, H. Arai, H. Tominaga, T. Kunugi, Bull. Chem. Soc. Jpn. 45 (1972) 607.
[30] L. Fu, C.H. Bartholomew, J. Catal. 92 (1985) 376.
[31] G.V. Schulz, J. Phys. Chem. Abst., B 29 (1935) 299.
[32] P.J. Flory, J. Am. Chem. Soc. 58 (1936) 1877.
[33] A. Dong, N. Ren, W. Yang, Y. Wang, Y. Zhang, D. Wang, J. Hu, Z. Gao, Y. Tang, Adv. Funct. Mater. 13 (2003) 943.
[34] X. Peng, M.C. Schlamp, A.V. Kadavannich, A.P. Alivisatos, J. Am. Chem. Soc. 119 (1997) 7019.
[35] N. Rem, Y. Yang, Y. Zhang, R. Wang, Y. Tang, J. Catal. 246 (2007) 215.
[36] V. Valtchev, Chem. Mater. 14 (2002) 956.
[37] S. Ikeda, S. Ishino, T. Harada, N. Okamoto, T. Sakata, H. Mori, S. Kuwabata, T. Torimoto, M. Matsumura, Angew. Chem. Int. Ed. 45 (2006) 7063.
[38] M. Miyamoto, T. Kamei, N. Nishiyama, Y. Egashira, K. Ueyama, Adv. Mater. 17 (2005) 1985.